Article

Cell PRESS

NMDA Receptor Ablation on Parvalbumin-Positive Interneurons Impairs Hippocampal Synchrony, Spatial Representations, and Working Memory

Tatiana Korotkova,[1,2,3] Elke C. Fuchs,[1,2,4] Alexey Ponomarenko,[1,3] Jakob von Engelhardt,[1,4] and Hannah Monyer[1,4,*]
[1]Department of Clinical Neurobiology, IZN, Im Neuenheimer Feld 364, 69120 Heidelberg, Germany
[2]These authors contributed equally to this work
[3]Present address: NeuroCure Cluster of Excellence Leibniz-Institute for Molecular Pharmacology (FMP), Charite Campus Mitte, Dorotheenstrasse 94, 10117 Berlin, Germany
[4]Present address: German Cancer Research Center (DKFZ), INF 280, 69120 Heidelberg, Germany
*Correspondence: monyer@urz.uni-hd.de

SUMMARY

Activity of parvalbumin-positive hippocampal interneurons is critical for network synchronization but the receptors involved therein have remained largely unknown. Here we report network and behavioral deficits in mice with selective ablation of NMDA receptors in parvalbumin-positive interneurons ($NR1^{PVCre-/-}$). Recordings of local field potentials and unitary neuronal activity in the hippocampal CA1 area revealed altered theta oscillations (5-10 Hz) in freely behaving $NR1^{PVCre-/-}$ mice. Moreover, in contrast to controls, in $NR1^{PVCre-/-}$ mice the remaining theta rhythm was abolished by the administration of atropine. Gamma oscillations (35-85 Hz) were increased and less modulated by the concurrent theta rhythm in the mutant. Positional firing of pyramidal cells in $NR1^{PVCre-/-}$ mice was less spatially and temporally precise. Finally, $NR1^{PVCre-/-}$ mice exhibited impaired spatial working as well as spatial short- and long-term recognition memory but showed no deficits in open field exploratory activity and spatial reference learning.

INTRODUCTION

Inhibitory interneurons can effectively control the excitability of principal cells (Buhl et al., 1994; Gulyas et al., 1993; Li et al., 1992; Sik et al., 1995) and thus play a critical role in cortical network function. A subset of GABAergic interneurons, namely fast-spiking, parvalbumin (PV)-positive cells are a major source of perisomatic inhibition onto pyramidal cells (Freund and Buzsaki, 1996) and are hence well suited to synchronize pyramidal cells during network oscillations.

The hippocampus displays several oscillatory synchronization states that correlate with distinct behavioral states (reviewed in Buzsaki [2002] and Fries et al. [2007]). Hippocampal network oscillations organize the firing of large neuronal populations at various time scales, thus providing conditions for adaptive operation of networks during information encoding, processing, and storage and are thought to be of functional relevance for cognitive processes (Gray and Singer, 1989; Harris et al., 2003; Wilson and McNaughton, 1993). During exploratory locomotion and paradoxical sleep in rodents, the hippocampus exhibits rhythmic field potentials at frequencies ranging from 5 to 10 Hz, i.e., theta rhythm (Vanderwolf, 1969; Winson, 1974) and concurrent gamma oscillations (Bragin et al., 1995; Colgin et al., 2009; Csicsvari et al., 2003; Montgomery et al., 2008), whereas high-frequency oscillations (140–200 Hz, "ripples") are characteristic for immobility and slow wave sleep (Buzsaki et al., 1992; Csicsvari et al., 1999; O'Keefe and Nadel, 1978). PV-positive cells are involved in cortical rhythmogenesis (Buzsaki and Eidelberg, 1983; Cardin et al., 2009; Fuchs et al., 2001; Klausberger et al., 2005; Sohal et al., 2009); however, the knowledge about their recruitment and the receptors involved therein has remained incomplete.

Like pyramidal cells, GABAergic interneurons, including PV-positive cells, receive excitatory input (Gulyas et al., 1999) that is mediated largely by glutamate receptors. Whereas the function of N-methyl-D-aspartic acid (NMDA) receptors in pyramidal cells is well established (Kauer et al., 1988; Nakazawa et al., 2004), their function in interneurons has remained elusive. Initial studies based on pharmacological approaches clearly revealed the importance of NMDA receptors in the hippocampus for memory formation (Kawabe et al., 1998; Morris et al., 1986). More recently developed genetic tools allowed the specific modification of NMDA receptors in defined cell types and brain regions. Furthermore, differential deletions of NMDA receptor subunits contributed to a better understanding of their functional role in hippocampus-dependent learning. In most studies so far, deletion of NMDA receptor subunits occurred in both pyramidal cells and interneurons in the whole brain or forebrain (Forrest et al., 1994; Mohn et al., 1999). Studies regarding cell type-specific NMDA receptor ablation focused so far on principal cells in the forebrain (Ebralidze et al., 1996; Ikeda et al., 1995; Sakimura et al., 1995; von Engelhardt et al., 2008) or different hippocampal subregions. The removal of the NR1 subunit in CA1, CA3, or dentate gyrus affected different forms of spatial learning, memory and modified spatial representations (McHugh et al., 1996; McHugh et al., 2007; Nakazawa et al., 2003; Niewoehner et al., 2007). A schizophrenia-like phenotype was described in two studies, in which NMDA receptors were
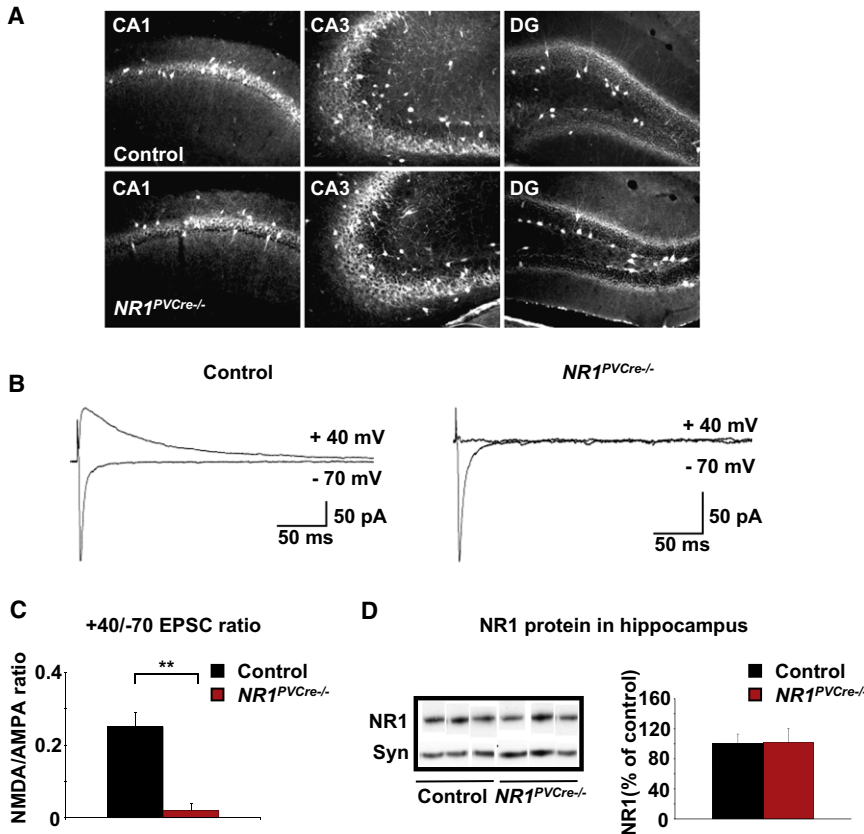
A

B

C

D

Figure 1. Ablation of NMDA Receptors in PV-Positive Interneurons

(A) Immunostaining for PV in hippocampal subregions of 4-month-old control (upper panels) and $NR1^{PVCre-/-}$ mice (lower panels) showed no alterations in the number and distribution of PV expression in CA1, CA3, and dentate gyrus (DG) of adult $NR1^{PVCre-/-}$ mice. See also Figure S1 and Table S1.

(B) Synaptic NMDA (+40 mV) and synaptic AMPA (−70 mV) EPSCs were evoked by extracellular stimulation and were recorded from PV-positive fast-spiking cells in slices of P50 (postnatal day 50) control (left) and $NR1^{PVCre-/-}$ (right) mice.

(C) Bar histogram represents average NMDA/AMPA ratios obtained from PV-positive fast-spiking cells in slices of P50 control (black bar, n = 14 cells from six animals) and $NR1^{PVCre-/-}$ (red bar, n = 15 cells from six animals) mice (mean ± standard error of the mean [SEM], p < 0.001).

(D) Overall NR1 subunit expression is not changed in hippocampi of adult control and $NR1^{PVCre-/-}$ mice. Representative western blot analysis showed similar NR1 protein levels in control and $NR1^{PVCre-/-}$ mice (three mice each) compared to synaptophysin (Syn) levels (left). Semiquantitative evaluation of protein levels from control and $NR1^{PVCre-/-}$ mice (n = 8 mice each, mean ± SEM, right).

modified either by an overall reduction of NR1 in the forebrain (Mohn et al., 1999) or by NR1 ablation in about half of the interneuron population in cortex and hippocampus (Belforte et al., 2010). However, the role of NMDA receptor-mediated excitation onto specific GABAergic neuron subpopulation for hippocampal network activities has not been studied.

Here we used genetically modified mice with NMDA receptor ablation restricted to PV-positive cells and studied the consequence of this manipulation in vivo at the network and behavioral level. We chose to target this interneuron subpopulation because its function for synchronous activity has been shown in numerous studies. To obtain complete ablation of NMDA receptors in PV-positive cells, we targeted the obligatory NMDA receptor subunit NR1 (Monyer et al., 1992). In $NR1^{PVCre-/-}$ mice, hippocampal local field potential and unitary recordings in the CA1 area in behaving mice revealed major changes in network synchronization and modified spatial representations that were accompanied by profound impairments in working and spatial recognition memory, leaving general exploratory behavior and spatial reference memory unaffected.

RESULTS

Selective Removal of NR1 Subunit from PV-Positive Interneurons

We generated $NR1^{PVCre-/-}$ mice by crossing PV-Cre mice (Fuchs et al., 2007) with mice carrying "floxed" NR1 alleles

(Niewoehner et al., 2007). Adult $NR1^{PVCre-/-}$ mice showed normal hippocampal morphology as revealed by immunostaining with the neuronal marker NeuN in coronal sections (see Figure S1 available online). The number of PV-positive cells in hippocampi of control and mutant mice was comparable (Figure 1A; Table S1). We confirmed the loss of NMDA receptor-mediated synaptic transmission onto PV-positive interneurons by whole-cell patch-clamp recordings in fast-spiking, putative PV-positive interneurons in the CA1 region in acute hippocampal slice preparations from P50-60 control and $NR1^{PVCre-/-}$ mice. The identification of the cells was based on their fast-spiking firing pattern, shape, and localization (Pawelzik et al., 2002). NMDA excitatory postsynaptic currents (EPSCs) were recorded at a holding potential of +40 mV and AMPA EPSCs were recorded at a holding potential of −70 mV. NMDA receptor-mediated currents were absent in 10 cells and strongly reduced in 5 cells compared to those of controls as indicated by a much smaller NMDA/AMPA ratio that was 0.25 ± 0.04 in control (n = 14 cells from six animals) and 0.02 ± 0.01 in $NR1^{PVCre-/-}$ mice (n = 15 cells from six animals, p < 0.001, Figures 1B and 1C). There was no significant difference in spontaneous AMPA receptor mediated EPSC properties (Table S2) indicating that the AMPA receptor mediated excitatory drive is unaltered in $NR1^{PVCre-/-}$ mice.

Western blot analysis of whole hippocampi revealed comparable levels of NR1 protein in adult $NR1^{PVCre-/-}$ and control mice (Figure 1D). Since PV-positive interneurons represent

a minor cell population, this result indicated that NR1 protein expression was not altered in other cell types.

Modified Hippocampal Theta Oscillations in *NR1*$^{PVCre−/−}$ Mice

Theta oscillations were recorded from the CA1 area during spontaneous exploration in a circular arena. The power of theta oscillations in str. pyramidale during exploration was significantly reduced in *NR1*$^{PVCre−/−}$ mice (cumulative power, n = 6 mice in each group, p < 0.01, Figure 2A). Theta rhythm was less stable (normalized amplitude variability, p < 0.05) and tended to be faster in the mutant (control 8.15 ± 0.03 Hz; *NR1*$^{PVCre−/−}$ 8.70 ± 0.04 Hz, p = 0.06). Alterations of theta oscillations were not due to differences in the running speed (control 7.4 ± 0.2 cm/s; *NR1*$^{PVCre−/−}$ 7.6 ± 0.2 cm/s, p = 0.4) and were present also during paradoxical sleep (Figure S2A). These local field potential (LFP) changes were accompanied by a reduced theta-rhythmicity of putative pyramidal cell and interneuron discharge as indicated by autocorrelograms (theta modulation index, pyramidal cells: control 0.45 ± 0.02; *NR1*$^{PVCre−/−}$ 0.34 ± 0.03, n = 72 pyramidal cells from five control and 64 pyramidal cells from five *NR1*$^{PVCre−/−}$ mice recorded with tetrodes, p < 0.01; interneurons: control 0.15 ± 0.01; *NR1*$^{PVCre−/−}$ 0.02 ± 0.01, n = 19 interneurons from five control and 30 interneurons from five *NR1*$^{PVCre−/−}$, p < 0.0001, Figures 2B and 2C) and interspike interval histograms (Figures S2B and S2C). Average firing rates of recorded units did not differ between genotypes (theta and non-theta states; pyramidal cells: 0.75 ± 0.05 versus 0.68 ± 0.06 Hz, p = 0.1; interneurons: 11.5 ± 0.7 versus 13.1 ± 0.8 Hz, p = 0.2).

The discharge of the vast majority of pyramidal cells was significantly modulated by theta rhythm in both genotypes (94.6% in controls and 91.4% in *NR1*$^{PVCre−/−}$), whereas only 53.3% of interneurons in *NR1*$^{PVCre−/−}$ mice (16 of 30) versus 100% (19 of 19) in controls were modulated by theta rhythm (p < 0.0005). Although the preferred phase of discharge of significantly modulated pyramidal cells displayed considerable variability in both genotypes (Figure 2D, see also Supplemental Results), the preferred firing of significantly modulated interneurons was close to the trough in control and *NR1*$^{PVCre−/−}$ mice (p > 0.5). The theta modulation of the discharge of the whole population of interneurons was dramatically decreased in *NR1*$^{PVCre−/−}$ mice (mean resultant vector length, control 0.24 ± 0.02; *NR1*$^{PVCre−/−}$ 0.07 ± 0.01, p < 0.0001, Figure 2D). The modulation of pyramidal cells was not significantly different between genotypes (control 0.16 ± 0.01; *NR1*$^{PVCre−/−}$ 0.14 ± 0.01, p = 0.3, Figure 2D).

Recordings with silicone probes in the CA1 area revealed a change in the laminar profile of theta oscillations in *NR1*$^{PVCre−/−}$ mice (n = 3 control and 3 *NR1*$^{PVCre−/−}$ mice, Figure 2E; Figure S2D). The characteristic maximum of the theta amplitude near the hippocampal fissure was absent in the mutant. The altered spatial distribution of theta currents in the mutant is reflected in the current-source density (CSD) maps (Figure 2F). Whereas in controls the theta-source in the pyramidal cell layer is associated with a large sink in the stratum lacunosum-moleculare (l-m, Brankack et al., 1993; Kamondi et al., 1998), in *NR1*$^{PVCre−/−}$ mice the two theta dipoles were of comparable magnitude. Thus group laminar CSD values in *NR1*$^{PVCre−/−}$ mice were distributed around the value computed for the str. pyramidale (p < 0.05 in control, p = 0.9 in *NR1*$^{PVCre−/−}$ mice, t test, Figure 2E). Theta oscillations were similarly highly coherent across hippocampal lamina in both genotypes (p < 0.05 in control, p < 0.01 in *NR1*$^{PVCre−/−}$ mice, Figure 2E).

The hippocampus displays two types of theta according to the sensitivity to the cholinergic blocker atropine (Buzsaki et al., 1986; Kramis et al., 1975). Since the features of theta oscillations in the mutant described above resemble those of the atropine-sensitive rhythm (Buzsaki et al., 1986; Hentschke et al., 2007), we studied their pharmacological characteristics. Administration of atropine led to a strong decrease of theta power in the mutant but not control mice (n = 5 control, n = 6 *NR1*$^{PVCre−/−}$ mice, p < 0.001, Figure 2G; Figure S3). The running speed (faster than 3 cm/s) after atropine administration did not differ (p = 0.99) between genotypes: 7.7 ± 0.6 cm/s in controls and 7.7 ± 1.0 cm/s in *NR1*$^{PVCre−/−}$ mice. The difference in the effect of atropine between controls and *NR1*$^{PVCre−/−}$ mice was also evident when comparing theta amplitudes between controls and mutants for the same running speed values, indicating that the atropine effect was independent of the running speed ($F_{(1,95)}$ = 70.92, p < 0.0001, ANCOVA, Figure 2H; for representative examples, see Figures S3 and S4). Tail-pinch induced theta oscillations after administration of urethane, known to elicit isolated atropine-sensitive theta (Kramis et al., 1975), did not differ between the two genotypes (theta amplitudes: $F_{(1,90)}$ = 0.01, p = 0.9; ANOVA; cumulative theta power: p = 0.2, n = 6 control, n = 5 *NR1*$^{PVCre−/−}$ mice, t test, Figure 2I). These findings collectively suggest that freely behaving *NR1*$^{PVCre−/−}$ mice display atropine-sensitive theta oscillations, whereas the atropine-resistant component is disrupted.

Augmented Hippocampal Gamma Oscillations in *NR1*$^{PVCre−/−}$ Mice

The pattern of the LFP signal in the CA1 area and its power spectrum indicated that gamma oscillations (35–85 Hz) during exploration were increased in *NR1*$^{PVCre−/−}$ mice (n = 6 mice in each group, cumulative power in the gamma band, p < 0.01, Figures 3A and 3B). Gamma oscillations were slightly faster (control 57.5 ± 0.3 Hz; *NR1*$^{PVCre−/−}$ 61.8 ± 0.9 Hz, p < 0.01) and their frequency was more temporally stable in the mutant (p < 0.05). To control for the contribution of remote (e.g., passively conducted from dentate gyrus) gamma currents generators to the recorded gamma LFP, we estimated various aspects of phase locking of the unitary activity to gamma oscillations during running. There were no significant differences between genotypes (pyramidal cells: control n = 72, *NR1*$^{PVCre−/−}$ n = 63; interneurons: control n = 22, *NR1*$^{PVCre−/−}$ n = 44, see Supplemental Results and Figure S5). The proportion of pyramidal cells and interneurons significantly modulated by gamma oscillations did not differ in controls and *NR1*$^{PVCre−/−}$ mice. Gamma phase preference histograms differed between controls and mutants for pyramidal cells (p < 0.00001, controls 60 units, mutants 56 units) but not for interneurons (p > 0.075, χ^2 test, controls 19 units, mutants 30 units). Interestingly, in *NR1*$^{PVCre−/−}$ mice the preferred group gamma-rhythmic discharge was significantly
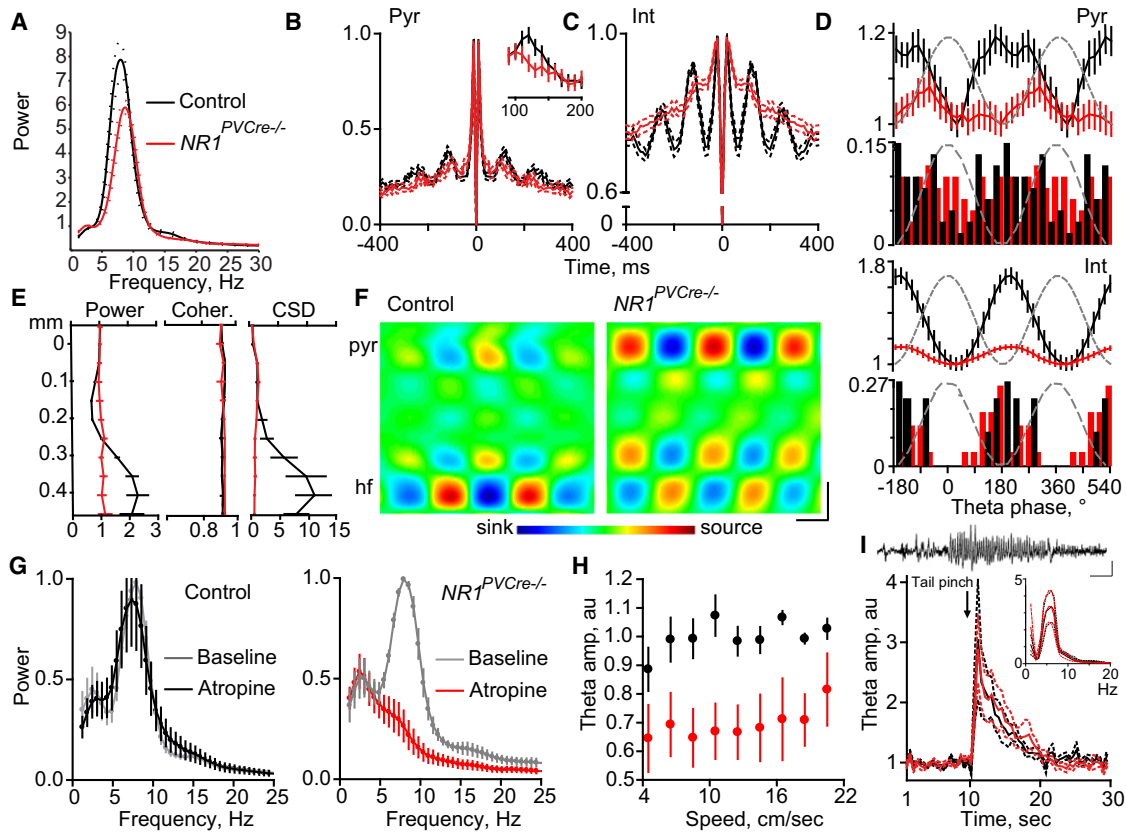
Figure 2. Altered Hippocampal Theta Oscillations in *NR1^PVCre−/−* Mice

(A) Power spectral density of theta oscillations (mean ± SEM) was reduced in *NR1^PVCre−/−* mice (control, black; *NR1^PVCre−/−*, red; n = 6 animals each, p < 0.01). LFP epochs with theta/delta power ratio ≥6.

(B and C) Autocorrelograms of pyramidal cells (B) and interneurons (C) indicate decreased theta rhythmicity of the discharge (p < 0.01 and p < 0.0001, respectively). Spike counts in 10 ms bins were normalized to the maximum for each cell. The inset shows the magnified fragment of the autocorrelogram corresponding to the theta band.

(D) Theta phase modulation of pyramidal cells (Pyr, upper two plots) and interneurons (Int, lower two plots). For each cell population theta phase modulation is depicted as the discharge of cells (top plot) and the preferred phase histogram for significantly modulated cells (bottom plot). The discharge of pyramidal cells was similarly modulated in control and mutants. Modulation of interneuron discharge during theta oscillation was lower in *NR1^PVCre−/−* mice (p < 0.0001). The firing probability is normalized to the minimal value of the respective group. Dotted sine-waves indicate theta reference cycles. Data are shown as mean ± SEM.

(E) The depth profile of theta oscillations computed from recordings with silicone probes was altered in *NR1^PVCre−/−* mice (mean ± SEM, control, black; *NR1^PVCre−/−*, red; n = 3 animals each). Reconstructed laminar positions of recording sites: str. pyramidale ~0 μm, stratum lacunosum-moleculare/hippocampal fissure 300–400 μm (see also Figure S2D). The typical increase of theta amplitude and CSD in controls in str. l-m is absent in *NR1^PVCre−/−* mice (left and right plots, normalized to values for str. pyramidale for each recording). Coherence of theta oscillations did not differ between genotypes (middle plot; reference site in str. pyramidale).

(F) Representative current-source density (CSD) maps (normalized to the maximum of each map). Note that in control (left) rhythmic sources and sinks were markedly stronger near the hippocampal fissure (hf) than in the pyramidal layer (pyr), whereas in *NR1^PVCre−/−* mice (right), sources and sinks in hf were comparable with those in the pyramidal cell layer. Scale bar represents 50 ms, 100 μm.

(G) Injection of atropine did not change significantly the power of theta oscillations in control (left panel, baseline-gray, atropine-black, n = 5 animals), but disrupted theta oscillations in *NR1^PVCre−/−* mice (right panel, baseline-gray, atropine-red, n = 6 animals, p < 0.001). Power spectra were computed for epochs with the running speed >5 cm/sec, normalized to baseline and shown as mean ± SEM. See also Figures S3 and S4. For the effect on gamma oscillations see Figure S5.

(H) Atropine-induced disruption of theta oscillations did not depend on running speed (posttreatment data; control, black; *NR1^PVCre−/−*, red; p < 0.0001). Data for each speed bin are presented as mean ± SEM. Au, arbitrary units obtained by the Hilbert transform.

(I) Remaining theta after urethane injection did not differ between control and *NR1^PVCre−/−* mice (n = 6 controls, 5 *NR1^PVCre−/−* mice). Upper trace is a representative trace of tail pinch-induced theta (scale bars represent 1 s, 1 mV). Neither mean amplitude (main plot) nor mean power (inset) of theta differed between control (black) and *NR1^PVCre−/−* (red) mice (p = 0.9 and p = 0.2, respectively).

more variable in pyramidal cells but was less variable in interneurons (circular concentration parameter, p < 0.01 and p < 0.05, respectively; see also Supplemental Results).

Gamma oscillations display rhythmic variation of magnitude and frequency within the concurrent theta cycle (Bragin et al., 1995; Buzsaki, 2002). The efficacy of this modulation was lower
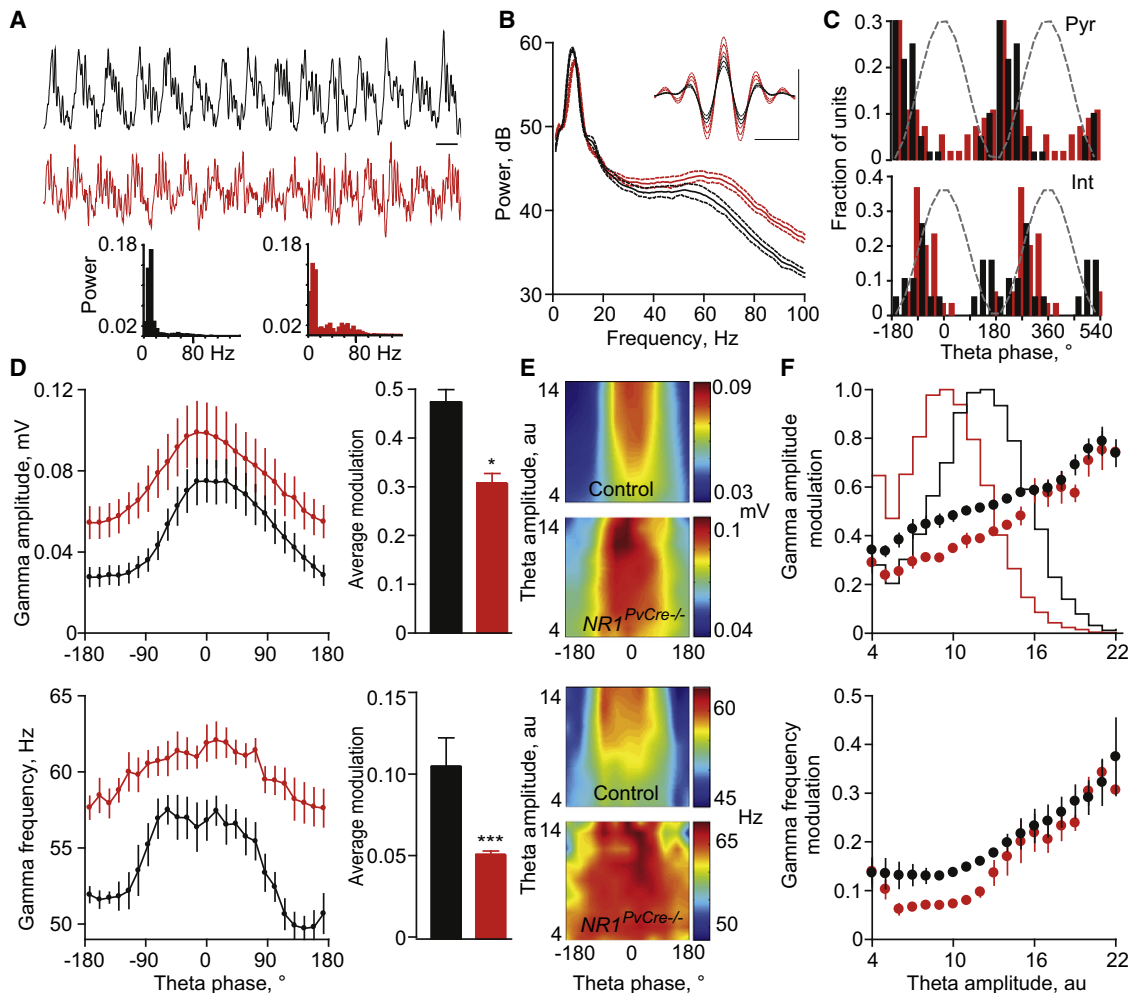
Figure 3. Increased Hippocampal Gamma Oscillations and Altered Coupling with Theta Oscillations in *NR1*^PVCre−/− Mice

(A) LFP signal traces (1–200 Hz bandwidth) illustrating augmented gamma oscillations in *NR1*^PVCre−/− (red) mice compared to controls (black). Scale bar represents 100 ms. The traces with theta cycles of similar amplitude were chosen to better illustrate the difference in gamma oscillations between *NR1*^PVCre−/− and control mice. Below: power spectra of these recording epochs.

(B) Power of gamma oscillations during running was increased in *NR1*^PVCre−/− mice (mean ± SEM, control, black; *NR1*^PVCre−/−, red; n = 6 animals each, p < 0.01). Inset: average gamma waveforms (mean ± SEM). Scale bars represent 20 ms, 100 μV.

(C) The preferred gamma phase histograms for significantly modulated pyramidal cells (Pyr, upper plot) and interneurons (Int, lower plot). In *NR1*^PVCre−/− mice the preferred group gamma-rhythmic discharge was significantly more variable in pyramidal cells (p < 0.01) but was less variable in interneurons (p < 0.05).

(D) Modulation of gamma amplitude (upper plot) and frequency (lower plot) was decreased in *NR1*^PVCre−/− mice (mean ± SEM; control, black; *NR1*^PVCre−/−, red; n = 6 animals each. *p < 0.05 and ***p < 0.0001, respectively).

(E) The modulation of gamma amplitude (upper plots) and frequency (lower plots) were reduced for theta cycles of different amplitudes (group average; y axis is scaled by the ratio to the delta band activity, au [arbitrary units]; color scale: red, maximal; blue, minimal values) in *NR1*^PVCre−/− mice compared to controls.

(F) The magnitude of the modulation of gamma amplitude (upper plot) and frequency (lower plot) was decreased across most, but not high-amplitude theta cycles. Histograms on upper plot represent amplitudes of theta cycles distribution in control (black) and *NR1*^PVCre−/− mice (red). Au, theta amplitude scaled by theta/delta power ratio. Data are shown as mean ± SEM.

in the mutant (average amplitude modulation coefficient: control 0.46 ± 0.03; *NR1*^PVCre−/− 0.31 ± 0.02, p < 0.05, average frequency modulation coefficient: control 0.1 ± 0.02; *NR1*^PVCre−/− 0.05 ± 0.002, p < 0.0001, Figure 3D). To assure that this effect did not result from the reduced theta per se, we analyzed the strength of coupling between theta and gamma rhythms for theta cycles that are similar in respects that influence gamma modulation, i.e., theta cycles of similar amplitudes

(Figure 3E). *NR1*^PVCre−/− mice displayed reduced gamma modulation across most, but not the highest-amplitude, theta cycles, which made up only ∼2% of all theta cycles (Figures 3E and 3F). Thus *NR1*^PVCre−/− mice display reduced theta phase-locking of gamma oscillations when average as well as individual theta cycles are considered.

Characteristics of fast ripple oscillations did not differ between controls (n = 6) and mutants (n = 6) (duration: control
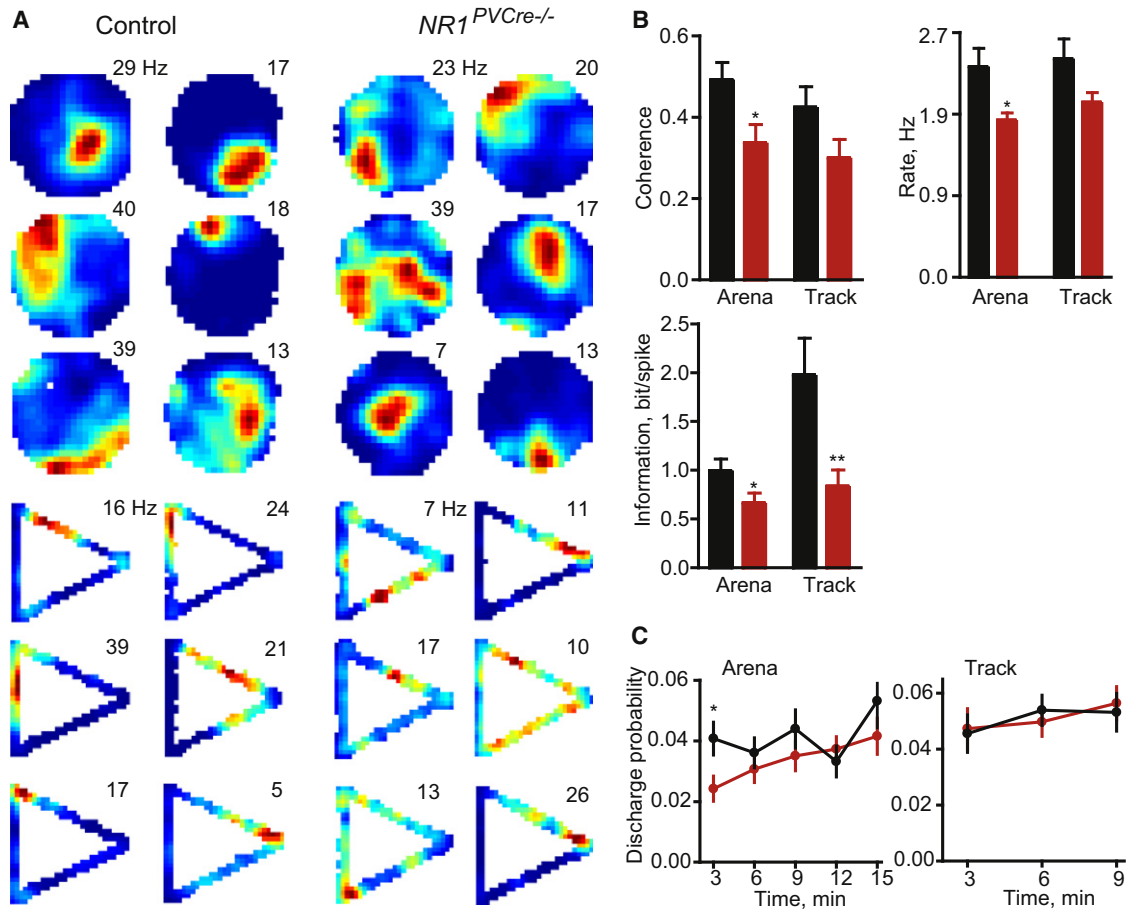
Figure 4. Spatial Representations in *NR1*^*PVCre−/−* Mice
(A) Representative firing-rate maps showing the discharge of control (left) and *NR1*^*PVCre-/-* (right) CA1 place cells in arena (upper plots) and triangle track (lower plots). Values were the peak firing rates of the respective place cells.
(B) Coherence, spatial information and mean firing rate in place field were decreased in *NR1*^*PVCre−/−* mice (mean ± SEM; control, black, NR1^*PVCre−/−*, red bars; *p < 0.05, **p < 0.01).
(C) The discharge probability (mean ± SEM) during the first 3 min of a session was reduced in *NR1*^*PVCre−/−* mice in the arena (*p < 0.05) but not on the linear track. The discharge probability increased within a session only in *NR1*^*PVCre−/−* mice (linear regression, p < 0.01).

100.5 ± 7.8 ms; *NR1*^*PVCre−/−* 105.3 ± 8.1 ms; frequency: control 178.3 ± 0.9 Hz; *NR1*^*PVCre-/* 177.3 ± 1.5 Hz; amplitude: control 698 ± 129 μV; *NR1*^*PVCre-/* 776 ± 118 μV). The efficacy of the neuronal discharge modulation by ripple oscillations was similar between genotypes (n = 62 pyramidal cells, 21 interneurons from five control mice and 136 pyramidal cells, 44 interneurons from five *NR1*^*PVCre−/−* mice, mean resultant vector length, p = 0.69 for pyramidal cells, p = 0.93 for interneurons).

Spatial Representations in *NR1*^*PVCre−/−* Mice
Positional firing of pyramidal cells in the CA1 area was studied during exploration of a circular arena (n = 43 cells from five control mice, n = 34 cells from 5 *NR1*^*PVCre−/−* mice) and on a linear track of triangular shape (n = 27 cells from five control mice, n = 29 cells from five *NR1*^*PVCre−/−* mice). The vast majority of pyramidal cells displayed spatially selective activity in both genotypes (Figure 4A). Isolated place fields of pyramidal cells were largely similar between genotypes when peak firing rate,

mean rate, field size, and the number of fields per cell were compared (Table 1).

However, pyramidal cells in the *NR1*^*PVCre−/−* mice conveyed lower spatial information than those in controls in the arena (p < 0.05) and on the track (p < 0.01) (Figure 4B). In *NR1*^*PVCre−/−* mice pyramidal cells had also significantly lower mean firing rates within place fields in the arena (p < 0.05). Firing of pyramidal cells in *NR1*^*PVCre−/−* mice was spatially less coherent in the arena (p < 0.05), indicating increased local spatial variance of the discharge. On the track spatial coherence tended to be reduced in the mutant (statistically not significant, p = 0.07). We next compared positional firing with reference both to environment (arena or track) and genotype to learn whether environment could account for differences observed for positional firing properties. Only spatial information was more affected in one environment (i.e., on the track) than in the other ($F_{(1,129)}$ = 6.1, p < 0.05, two-way ANOVA) but not spatial coherence (p > 0.84) and mean firing rate (p > 0.74).

Table 1. Properties of CA1 Place Cells

	Arena, Control	Arena, $NR1^{PVCre-/-}$	Track, Control	Track, $NR1^{PVCre-/-}$
Peak rate, Hz	18.56 ± 1.92	15.42 ± 1.73	15.11 ± 1.71	12.01 ± 1.07
Mean rate (MR), Hz	1.02 ± 0.10	0.82 ± 0.11	1.06 ± 0.16	1.2 ± 0.18
Field size, cm2	397.48 ± 42.16	408.99 ± 59.69	250.52 ± 38.08	512.06 ± 152.94
N fields	1.91 ± 0.18	1.53 ± 0.14	2.67 ± 0.25	2.62 ± 0.26
MR in field, Hz	2.32 ± 0.20	1.73 ± 0.08[a]	2.41 ± 0.21	1.93 ± 0.11
Spatial information	1.0 ± 0.11	0.67 ± 0.10[a]	1.98 ± 0.28	0.84 ± 0.17[b]
Coherence	0.49 ± 0.04	0.34 ± 0.05[a]	0.43 ± 0.05	0.3 ± 0.05

[a] $p < 0.05$.
[b] $p < 0.01$.

The temporal analysis of the discharge in place fields within individual sessions revealed that during the first 3 min of a session, the discharge probability in place fields in $NR1^{PVCre-/-}$ mice is reduced in the arena ($p < 0.05$) but not on the track (Figure 4C). Whereas in controls the firing probability in place fields did not change within a session, the discharge probability in $NR1^{PVCre-/-}$ mice increased within the session (linear regression (Runs test), Pearson r = 0.99, $p < 0.01$).

Behavioral Analysis of $NR1^{PVCre-/-}$ Mice

The behavioral analysis comprised a battery of tests to assess exploratory behavior, hippocampus-dependent learning, and memory. We compared the exploratory activity in response to novel stimuli in the open field arena. Compared to control mice, $NR1^{PVCre-/-}$ mice showed no difference in the number of squares crossed on day 1 and day 2 of testing (Figure 5A). $NR1^{PVCre-/-}$ mice performed fewer rearings on day 1 (number of rearings day 1: control 45.9 ± 3.7, n = 19; $NR1^{PVCre-/-}$ 31.8 ± 3.3, n = 17; $F_{(1,35)} = 7.8$, $p = 0.008$), but both genotypes reared to a similar extent on the second day.

Mice were exposed to a plastic toy and an unfamiliar mouse in the open field arena for 5 min. Both the toy and the mouse were confined to small, wired cages. Control and $NR1^{PVCre-/-}$ mice expressed a clear preference for the unfamiliar mouse, and there were no differences of overall exploratory activity (Figure 5B).

We analyzed the memory capability for new objects with only a short delay between the training and the test phase of the task. The measurement of rodents' ability to recognize novel objects (Alarcon et al., 2004; Rampon et al., 2000) is based on their natural exploratory behavior and their ability to remember previously encountered objects. During the 5 min training phase $NR1^{PVCre-/-}$ mice spent slightly less time exploring the two different objects (control 17.8 ± 3 s, n = 18; $NR1^{PVCre-/-}$ 12 ± 3.4 s, n = 13, H = 4.1, p = 0.043). The total time exploring the familiar object and the new object during the test phase did not differ between the genotypes (control 12.9 ± 2 s; $NR1^{PVCre-/-}$ 15.7 ± 5.7 s). However, only control mice expressed a preference for the new object (discrimination ratio control 0.71 ± 0.02, $NR1^{PVCre-/-}$ 0.46 ± 0.05, H = 11.9, $p < 0.001$, Figure 5C).

Spatial reference memory was not affected in $NR1^{PVCre-/-}$ mice in contrast to spatial working memory that was profoundly
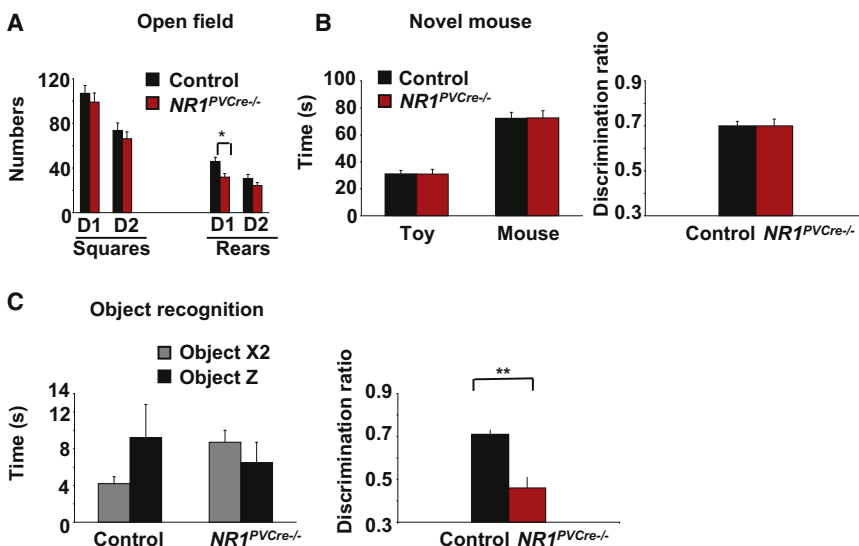
Figure 5. Impaired Object Recognition Memory in $NR1^{PVCre-/-}$ Mice

(A) $NR1^{PVCre-/-}$ crossed a similar number of squares in an open field test. They performed fewer rearings on day 1 than control animals ($p < 0.01$), but there was no difference in the number of rearings on day 2. The test was performed twice on two consecutive days (control n = 19, $NR1^{PVCre-/-}$ n = 17, D1 = day 1, D2 = day 2).
(B) Mice were exposed to a plastic toy and an unfamiliar mouse. Both genotypes spent more time exploring the unfamiliar mouse than the toy (control n = 15, $NR1^{PVCre-/-}$ n = 14) during 5 min. The discrimination ratio [unfamiliar mouse object/ (unfamiliar mouse + toy)] revealed a strong preference of both genotypes for the unfamiliar mouse.
(C) After a 5 min training phase with two different objects (object X1 and Y1), a novel object (Z) substituted one of the familiar objects and a duplicate for the other familiar object (X2) was used to prevent olfactory cues. The time spent with the two objects during the 5 min test phase is depicted in the left panel. A discrimination ratio [new object/

(new + familiar object)] was calculated for the time spent with the new object Z and the familiar object X2 (chance performance 0.50). Only control animals (n = 18) expressed a preference for the new object Z, $NR1^{PVCre-/-}$ mice (n = 13) performed at chance level (right panel, $p < 0.001$). Each column represents mean ± SEM.
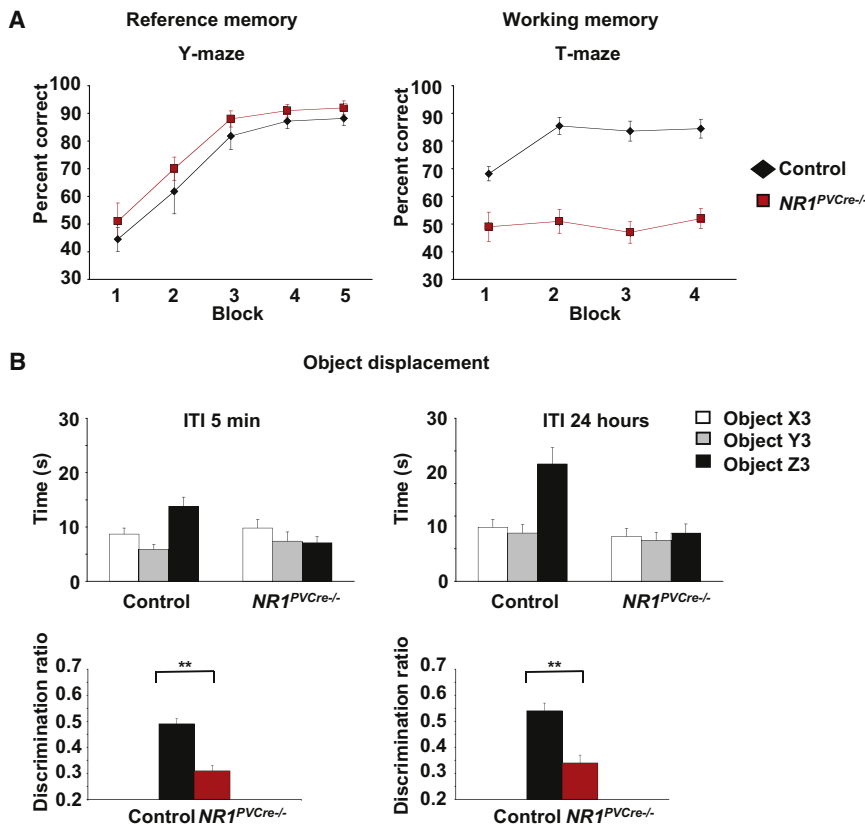
Figure 6. Impaired Spatial Working and Recognition Memory in *NR1^{PVCre−/−}* Mice

(A) Mean percent correct responses (±) SEM during acquisition of an appetitive hippocampus-dependent spatial reference memory task on the elevated Y-maze for control (black diamonds, n = 11) and *NR1^{PVCre−/−}* mice (red squares, n = 10) (left panel). Mean percent correct responses (±) SEM during hippocampus-dependent spatial nonmatching to place testing on the elevated T-maze for control (black diamonds, n = 11) and *NR1^{PVCre−/−}* mice (red squares, n = 10) (right panel). *NR1^{PVCre−/−}* mice perform at chance level (50% correct, p < 0.001). Each block consists of 10 trials per mouse.

(B) The object displacement task was used to assess short- and long-term memory for the location of an object. The mice performed the test phase 5 min (control n = 17, *NR1^{PVCre−/−}* n = 14) or 24 hr (control n = 12, *NR1^{PVCre−/−}* n = 13) after training; during the test phase object Z3 was displaced. The time spent with the three objects X3, Y3, and Z3 during the test phase is depicted in upper panels. Lower panels: A discrimination ratio [displaced object/(all three objects)] was calculated for the time spent with the displaced object Z3 and the two other objects X3 and Y3 (chance performance 0.30). Only control mice showed a preference for the displaced object after a delay of 5 min and 24 hr (p < 0.001). Each column represents mean ± SEM.

impaired. In *NR1^{PVCre−/−}* mice spatial reference memory was assessed using an appetitive task on an elevated Y-maze. Notably, both mutant and control animals learned the task at a similar rate and reached the same high level of performance (control 88.2 ± 2.6%, n = 11; *NR1^{PVCre−/−}* 91 ± 2.5%, n = 10, Figure 6A). Spatial working memory was analyzed using hippocampus-dependent rewarded alternation (non-matching-to-place) on the T-maze (Rawlins and Olton, 1982). Control mice performed well from the beginning on this rewarded alternation task, attaining a choice accuracy of 80.5 ± 1.8% (n = 11). In contrast, *NR1^{PVCre−/−}* mice were alternating at chance level (49.8% ± 1.9%, n = 10; $F_{(1,20)}$ = 132.7, p < 0.001, Figure 6A).

To analyze short- and long-term spatial recognition memory, a short intertrial interval (5 min) and a long intertrial interval (24 hr) between training and test phase were used (Figure 6B) in the object displacement task. During the first 5 min training phase, *NR1^{PVCre−/−}* mice spent significantly less time exploring the objects compared to control mice (time spent with objects X, Y, and Z: control 32.1 ± 2.3 s; *NR1^{PVCre−/−}* 24.6 ± 2.3 s; $F_{(1,55)}$ = 5.3, p = 0.025). There was no difference in exploration time between the two genotypes during the second 5 min training phase. In the test phase one object (object Z3) was displaced. The total amount of time spent with the three objects was the same for control and *NR1^{PVCre−/−}* mice after the short 5 min delay time (time spent with objects X3, Y3, and Z3: control 28.4 ± 3.4 s, n = 17; NR1^{PVCre−/−} 24.2 ± 3.7 s, n = 14). Interestingly, the mutants spent less time exploring the three objects after the 24 hr delay

(time spent with objects X3, Y3, and Z3: control 33.8 ± 4.4 s, n = 12; *NR1^{PVCre−/−}* 20.6 ± 2.9 s, n = 13; H = 5.61, p = 0.018). To compare recognition memory between the genotypes, we calculated discrimination ratios for the short and long intertrial interval. Only control mice spent significantly more time with the displaced object Z3 after an interval of 5 min ($F_{(1,30)}$ = 34.8; P < 0.001) or 24 hr ($F_{(1,24)}$ = 29.2; p < 0.001) (Figure 6B).

DISCUSSION

Here we show that selective ablation of NMDA receptors in PV-positive interneurons leads to deficits at the cellular, network and behavioral level. As we reported previously, cell type-selective specificity of transgenic *PV-Cre* mice assured the expression of Cre-recombinase in PV-positive cells (Fuchs et al., 2007). As Cre-recombinase expression under the control of the PV promoter is not detectable before the second postnatal week, early development was not affected. The deletion of the NR1 subunit led to a selective loss of synaptic NMDA receptor-mediated currents in PV-positive fast-spiking cells in P50-60 old mice. *NR1^{PVCre−/−}* mice are thus well suited to investigate the significance of NMDA receptor-mediated input onto PV-positive interneurons in hippocampal processing.

Hippocampal Network Oscillations in *NR1^{PVCre−/−}* Mice

Theta rhythm, a major hallmark of hippocampal population activity during locomotion and paradoxical sleep, is assumed

to be a carrier of mnemonic processes (see Buzsaki [2002] for review; Lisman and Idiart, 1995; Raghavachari et al., 2001). The origin of theta rhythm and current generators from specific hippocampal and extrahippocampal regions has been the focus of many studies (Kocsis et al., 1999; Montgomery et al., 2008), but the contribution of different cell types, neurotransmitters and receptors involved has remained largely unknown. Although there is no doubt that fast-spiking interneurons are crucially involved in rhythmogenesis, and NMDA receptor blockers affect hippocampal rhythms (Hakami et al., 2009; Roopun et al., 2008), the genetic approach taken here allowed a direct investigation whether and how NMDA receptors on PV-positive interneurons contribute to network oscillations. We demonstrate that the loss of NMDA receptors in PV interneurons differentially affects hippocampal theta and gamma but not ripple oscillations.

A major finding in this study is that ablation of NMDA receptors on PV-positive interneurons results in diminished theta oscillations accompanied by altered theta-frequency coordination of neuronal activity. Interestingly, reducing the excitatory drive on PV-positive interneurons by ablating the GluR-A AMPA receptor subunit *GluR-A*$^{PVCre-/-}$ did not affect theta rhythm but led to alteration of hippocampal synchrony during ~200 Hz ripple oscillations (Racz et al., 2009). Furthermore, the lack of NMDA receptor expression in PV-positive cells selectively abolishes atropine-resistant but not atropine-sensitive theta rhythm. The existence of the two types of theta rhythm in the hippocampus has long been known (Kramis et al., 1975), but the underlying mechanisms and functions have not been fully elucidated. Atropine-resistant theta is reported to be movement-related whereas atropine-sensitive theta is associated with sensory processing during resting immobility in rats (Bland, 1986; Bland and Oddie, 2001). The atropine-resistant rhythm is eliminated in vivo by the anesthetic urethane (Kramis et al., 1975), the actions of which include the reduction of NMDA currents (Hara and Harris, 2002). NMDA receptor antagonists rendered laminar features of theta oscillations in rats similar to those observed under urethane anesthesia (Soltesz and Deschenes, 1993) and blocked atropine-resistant theta in hippocampal slices (Gillies et al., 2002). The suggested network mechanisms of the atropine-resistant rhythm include a role for both excitatory (i.e., NMDA receptor-mediated; Horvath et al., 1988; Buzsaki, 2002) and inhibitory mechanisms (Gillies et al., 2002; Goutagny et al., 2009). In this study, we show that the selective ablation of NMDA receptors on PV-positive neurons sufficed to abolish this rhythm.

Along with hippocampus, medial septum and entorhinal cortex are also necessary for the generation of atropine-resistant theta in vivo (Buzsaki et al., 1983; Freund and Antal, 1988; Vanderwolf and Leung, 1983). Lesions of the medial septum-diagonal band of Broca, lead to abolished theta rhythm in hippocampus (Petsche et al., 1962) and to decreased theta rhythm in the entorhinal cortex (Jeffery et al., 1995; Mitchell et al., 1982). Medial septum comprises both atropine-sensitive and atropine-insensitive PV-positive neurons (Stewart and Fox 1990). Theta rhythmicity is also conveyed to hippocampal pyramidal cells and interneurons by entorhinal cortex afferents (Kiss et al., 1996; Sik et al., 1995). Both in the medial septum and in

the entorhinal cortex Cre-expression can be detected in a subpopulation of PV-positive cells in *NR1*$^{PVCre-/-}$ mice (see Figure S6). We can thus not exclude that deletion of NR1 subunit in PV-positive cells in these brain regions also contribute to the phenotype described here. Altogether our results suggest that atropine-resistant theta in the hippocampus strongly relies on NMDA receptor signaling in PV-positive neurons.

Here we describe an isolated atropine-sensitive theta in genetically modified freely moving mice. An inverse phenotype regarding the differential effect on the two theta rhythms, i.e., a lack of atropine-sensitive theta rhythm but preserved atropine-resistant rhythm is found in phospholipase C-β1 knockout mice (Shin et al., 2005).

Altered theta rhythm is associated in *NR1*$^{PVCre-/-}$ mice with facilitated LFP gamma oscillations. Our results extend previous observations according to which hippocampal gamma oscillations were increased after systemic injection of phencyclidine (Ma and Leung, 2000), an NMDA receptor blocker known to also suppress atropine-resistant theta (Vanderwolf and Leung, 1983). Theta rhythmicity organizes gamma frequency dynamics of neuronal populations (Bragin et al., 1995; Colgin et al., 2009; Mizuseki et al., 2009; Rotstein et al., 2005; Sirota et al., 2008; Tort et al., 2008; Wulff et al., 2009). Gamma oscillations disintegrate in a computational model when the overall drive to inhibitory cells becomes strong (Borgers et al., 2008). One might expect the opposite in *NR1*$^{PVCre-/-}$ mice, in which the reduced excitatory input to interneurons relative to that onto pyramidal cells could result in the generation of gamma oscillations throughout the theta cycle. The other altered feature in *NR1*$^{PVCre-/-}$ mice, namely selectively reduced gamma modulation for theta cycles of lower magnitude, is in line with a model and experimental data in vitro suggesting that the strength of theta-synchronization of basket cells accounts for gamma modulation (Gloveli et al., 2005). In addition, theta rhythmicity of gamma oscillations might require NMDA receptor-mediated input onto PV-positive cells during theta oscillations of lower and intermediate magnitude whereas other (e.g., voltage dependent) mechanisms operate during theta cycles of large amplitude. Theta/gamma coordination is proposed to assist encoding preserving serial order of inputs, thus providing a way of representing items in short-term and working memory (Lisman, 2005; Lisman and Buzsaki, 2008; Lisman and Idiart, 1995). Hence, deficits in the coupling of the oscillations could lead to alteration in the hippocampal information processing.

The reliability of spatial representations in the hippocampus (O'Keefe and Nadel, 1978) strongly depends on intact signaling via NMDA receptors (McHugh et al., 1996; McHugh et al., 2007; Nakazawa et al., 2002). In *NR1*$^{PVCre-/-}$ mice, positional firing, though largely retained, was less spatially and temporally robust. Interestingly, the temporal pattern of place fields in the familiar environment in mutants is more reminiscent of that reported for rodents in a novel environment (Frank et al., 2004) than to temporally uniform firing in controls. These alterations were not accompanied by an altered performance in spatial reference memory paradigms, but were associated with deficits in spatial working-memory tasks. Our findings suggest that precision of hippocampal spatial representations is decreased when NMDARs on PV-positive cells are absent.

Hippocampus-Dependent Behavior in *NR1*^{PVCre−/−} Mice

The behavioral phenotype of *NR1*^{PVCre−/−} mice is characterized by the impairment of working memory, short- and long-term spatial recognition memory but unaltered reference memory. We took recourse to a battery of tests that are believed to assess hippocampus-dependent behavior but we cannot exclude that other cortical regions are involved. Certain deficits are reminiscent of the ones found in knockout mice with NMDA receptor ablation in larger cell populations, indicating that in those mutants some deficits may have resulted at least in part from NMDA receptor ablation in interneuron populations.

The behavioral phenotype of *NR1*^{PVCre−/−} mice differs from that reported in mice with NR2 subunit deletion in forebrain neurons. Interestingly, global ablation of NR2A resulted in a behavioral phenotype that was milder than that observed here in *NR1*^{PVCre−/−} mice (Sakimura et al., 1995). Although impaired, the performance on the T-maze of mice lacking NR2A was significantly above chance level, whereas *NR1*^{PVCre−/−} mice performed consistently at chance. The phenotype of *NR1*^{PVCre−/−} mice differs from that of mice having NR2B deleted in pyramidal cells that exhibited working and reference memory alterations (von Engelhardt et al., 2008).

Mouse mutants with region-specific ablations of NMDA receptors in pyramidal cells provided insight regarding the complex and differential role of these receptors in defined hippocampal subregions (Nakazawa et al., 2004). Thus, NMDA receptor knockout in CA1 resulted in impaired reference memory (McHugh et al., 1996) whereas ablation in CA3 or DG resulted in working memory deficits (McHugh et al., 2007; Niewoehner et al., 2007). As far as comparisons go, considering differences in testing conditions in the different studies, the behavioral phenotype of *NR1*^{PVCre−/−} mice resembles that of mice lacking NMDA receptors in the CA3 region. Disruption of NMDA receptor function in CA3 either by genetic or pharmacological means was associated with working memory but not reference memory deficits (Lee and Kesner, 2002; Nakazawa et al., 2002; Nakazawa et al., 2003). Similarly, in *NR1*^{PVCre−/−} mice the profound deficit in tasks involving rapid one-trial spatial learning (T-maze, object displacement) contrasts with the normal performance in tasks probing spatial reference learning over many trials (Y-maze).

Of note are similar behavioral deficits, albeit less pronounced, in mice with reduced AMPA-receptor currents in PV-positive interneurons (Fuchs et al., 2007). Thus, interfering with NMDA- or AMPA-receptors on PV-positive cells results in spatial working memory deficits revealing the crucial role of this cell population in orchestrating network activity and memory performance.

Although dysfunction or loss of PV-positive cells is linked with schizophrenia (Lewis et al., 2005; Lodge et al., 2009), our study did not indicate abnormal social behavior in *NR1*^{PVCre−/−} mice. Our results also differ in this respect from those reported by Belforte and colleagues who observed a "schizophrenia-like" phenotype in mice with NMDA receptor deletion in about half of cortical and hippocampal interneurons (Belforte et al., 2010). This work complements a previous study suggesting that reduced NMDA receptor expression was associated with a "schizophrenia-like" behavioral phenotype (Mohn et al., 1999). In the Belforte et al. (2010) study, NMDA receptors were ablated in about 50% of GABAergic interneurons, which comprise mainly PV-positive cells but also somatostatin- and NPY-positive subpopulations. This may, at least in part, explain differences regarding the social behavior of these mice compared to *NR1*^{PVCre−/−} mice.

In summary, the behavioral data along with alterations of hippocampal processing during theta oscillations highlight the functional significance of NMDA receptors in PV-positive cells in the collective operation of hippocampal networks, spatial representations and for spatial working memory.

EXPERIMENTAL PROCEDURES

All procedures involving experimental mice had ethical approval from the Regierungspräsidium Karlsruhe, Germany.

Western Blot Analysis, In Situ Hybridization, Immunohistochemistry, and Histology

These methods involved standard procedures described in Supplemental Experimental Procedures.

Electrophysiology in Slices

Electrophysiological analyses were performed on 250 μm transverse hippocampal slices of *NR1*^{PVCre−/−} mice and control littermates (see Supplemental Experimental Procedures).

Behavioral Analysis

Behavioral experiments (see Supplemental Experimental Procedures) were conducted with age-matched *NR1*^{PVCre−/−} mice and control littermates.

In Vivo Recordings

Wire electrodes (tetrodes or arrays of single wires) or silicone probes were implanted above the hippocampus and subsequently positioned in the CA1 pyramidal cell layer, using LFP and unitary activity as a reference. Unitary and LFP signals were acquired during exploratory behavior and sleep (see Supplemental Experimental Procedures).

SUPPLEMENTAL INFORMATION

Supplemental Information includes Supplemental Experimental Procedures, six figures, and one table and can be found with this article online at doi:10.1016/j.neuron.2010.09.017.

REFERENCES

Alarcon, J.M., Malleret, G., Touzani, K., Vronskaya, S., Ishii, S., Kandel, E.R., and Barco, A. (2004). Chromatin acetylation, memory, and LTP are impaired in CBP+/− mice: A model for the cognitive deficit in Rubinstein-Taybi syndrome and its amelioration. Neuron *42*, 947–959.

Belforte, J.E., Zsiros, V., Sklar, E.R., Jiang, Z., Yu, G., Li, Y., Quinlan, E.M., and Nakazawa, K. (2010). Postnatal NMDA receptor ablation in corticolimbic interneurons confers schizophrenia-like phenotypes. Nat. Neurosci. *13*, 76–83.

Bland, B.H. (1986). The physiology and pharmacology of hippocampal formation theta rhythms. Prog. Neurobiol. *26*, 1–54.

Bland, B.H., and Oddie, S.D. (2001). Theta band oscillation and synchrony in the hippocampal formation and associated structures: The case for its role in sensorimotor integration. Behav. Brain Res. *127*, 119–136.

Borgers, C., Epstein, S., and Kopell, N.J. (2008). Gamma oscillations mediate stimulus competition and attentional selection in a cortical network model. Proc. Natl. Acad. Sci. USA *105*, 18023–18028.

Bragin, A., Jando, G., Nadasdy, Z., Hetke, J., Wise, K., and Buzsaki, G. (1995). Gamma (40-100 Hz) oscillation in the hippocampus of the behaving rat. J. Neurosci. *15*, 47–60.

Brankack, J., Stewart, M., and Fox, S.E. (1993). Current source density analysis of the hippocampal theta rhythm: Associated sustained potentials and candidate synaptic generators. Brain Res. *615*, 310–327.

Buhl, E.H., Halasy, K., and Somogyi, P. (1994). Diverse sources of hippocampal unitary inhibitory postsynaptic potentials and the number of synaptic release sites. Nature *368*, 823–828.

Buzsaki, G. (2002). Theta oscillations in the hippocampus. Neuron *33*, 325–340.

Buzsaki, G., and Eidelberg, E. (1983). Phase relations of hippocampal projection cells and interneurons to theta activity in the anesthetized rat. Brain Res. *266*, 334–339.

Buzsaki, G., Leung, L.W., and Vanderwolf, C.H. (1983). Cellular bases of hippocampal EEG in the behaving rat. Brain Res. *287*, 139–171.

Buzsaki, G., Czopf, J., Kondakor, I., and Kellenyi, L. (1986). Laminar distribution of hippocampal rhythmic slow activity (RSA) in the behaving rat: Current-source density analysis, effects of urethane and atropine. Brain Res. *365*, 125–137.

Buzsaki, G., Horvath, Z., Urioste, R., Hetke, J., and Wise, K. (1992). High-frequency network oscillation in the hippocampus. Science *256*, 1025–1027.

Cardin, J.A., Carlen, M., Meletis, K., Knoblich, U., Zhang, F., Deisseroth, K., Tsai, L.H., and Moore, C.I. (2009). Driving fast-spiking cells induces gamma rhythm and controls sensory responses. Nature *459*, 663–667.

Colgin, L.L., Denninger, T., Fyhn, M., Hafting, T., Bonnevie, T., Jensen, O., Moser, M.B., and Moser, E.I. (2009). Frequency of gamma oscillations routes flow of information in the hippocampus. Nature *462*, 353–357.

Csicsvari, J., Hirase, H., Czurko, A., Mamiya, A., and Buzsaki, G. (1999). Fast network oscillations in the hippocampal CA1 region of the behaving rat. J. Neurosci. *19*, RC20.

Csicsvari, J., Jamieson, B., Wise, K.D., and Buzsaki, G. (2003). Mechanisms of gamma oscillations in the hippocampus of the behaving rat. Neuron *37*, 311–322.

Ebralidze, A.K., Rossi, D.J., Tonegawa, S., and Slater, N.T. (1996). Modification of NMDA receptor channels and synaptic transmission by targeted disruption of the NR2C gene. J. Neurosci. *16*, 5014–5025.

Forrest, D., Yuzaki, M., Soares, H.D., Ng, L., Luk, D.C., Sheng, M., Stewart, C.L., Morgan, J.I., Connor, J.A., and Curran, T. (1994). Targeted disruption of NMDA receptor 1 gene abolishes NMDA response and results in neonatal death. Neuron *13*, 325–338.

Frank, L.M., Stanley, G.B., and Brown, E.N. (2004). Hippocampal plasticity across multiple days of exposure to novel environments. J. Neurosci. *24*, 7681–7689.

Freund, T.F., and Antal, M. (1988). GABA-containing neurons in the septum control inhibitory interneurons in the hippocampus. Nature *336*, 170–173.

Freund, T.F., and Buzsaki, G. (1996). Interneurons of the hippocampus. Hippocampus *6*, 347–470.

Fries, P., Nikolic, D., and Singer, W. (2007). The gamma cycle. Trends Neurosci. *30*, 309–316.

Fuchs, E.C., Doheny, H., Faulkner, H., Caputi, A., Traub, R.D., Bibbig, A., Kopell, N., Whittington, M.A., and Monyer, H. (2001). Genetically altered AMPA-type glutamate receptor kinetics in interneurons disrupt long-range synchrony of gamma oscillation. Proc. Natl. Acad. Sci. USA *98*, 3571–3576.

Fuchs, E.C., Zivkovic, A.R., Cunningham, M.O., Middleton, S., Lebeau, F.E., Bannerman, D.M., Rozov, A., Whittington, M.A., Traub, R.D., Rawlins, J.N., and Monyer, H. (2007). Recruitment of parvalbumin-positive interneurons determines hippocampal function and associated behavior. Neuron *53*, 591–604.

Gillies, M.J., Traub, R.D., LeBeau, F.E., Davies, C.H., Gloveli, T., Buhl, E.H., and Whittington, M.A. (2002). A model of atropine-resistant theta oscillations in rat hippocampal area CA1. J. Physiol. *543*, 779–793.

Gloveli, T., Dugladze, T., Rotstein, H.G., Traub, R.D., Monyer, H., Heinemann, U., Whittington, M.A., and Kopell, N.J. (2005). Orthogonal arrangement of rhythm-generating microcircuits in the hippocampus. Proc. Natl. Acad. Sci. USA *102*, 13295–13300.

Goutagny, R., Jackson, J., and Williams, S. (2009). Self-generated theta oscillations in the hippocampus. Nat. Neurosci. *12*, 1491–1493.

Gray, C.M., and Singer, W. (1989). Stimulus-specific neuronal oscillations in orientation columns of cat visual cortex. Proc. Natl. Acad. Sci. USA *86*, 1698–1702.

Gulyas, A.I., Miles, R., Sik, A., Toth, K., Tamamaki, N., and Freund, T.F. (1993). Hippocampal pyramidal cells excite inhibitory neurons through a single release site. Nature *366*, 683–687.

Gulyas, A.I., Megias, M., Emri, Z., and Freund, T.F. (1999). Total number and ratio of excitatory and inhibitory synapses converging onto single interneurons of different types in the CA1 area of the rat hippocampus. J. Neurosci. *19*, 10082–10097.

Hakami, T., Jones, N.C., Tolmacheva, E.A., Gaudias, J., Chaumont, J., Salzberg, M., O'Brien, T.J., and Pinault, D. (2009). NMDA receptor hypofunction leads to generalized and persistent aberrant gamma oscillations independent of hyperlocomotion and the state of consciousness. PLoS ONE *4*, e6755.

Hara, K., and Harris, R.A. (2002). The anesthetic mechanism of urethane: The effects on neurotransmitter-gated ion channels. Anesth. Analg. *94*, 313–318.

Harris, K.D., Csicsvari, J., Hirase, H., Dragoi, G., and Buzsaki, G. (2003). Organization of cell assemblies in the hippocampus. Nature *424*, 552–556.

Hentschke, H., Perkins, M.G., Pearce, R.A., and Banks, M.I. (2007). Muscarinic blockade weakens interaction of gamma with theta rhythms in mouse hippocampus. Eur. J. Neurosci. *26*, 1642–1656.

Horvath, Z., Kamondi, A., Czopf, J., Bliss, T.V.P., and Buzsaki, G. (1988). NMDA receptors may be involved in generation of hippocampal theta rhythm. In Synaptic Plasticity in the Hippocampus, H.L. Haas and G. Buzsaki, eds. (Berlin: Springer-Verlag), p. 45.

Ikeda, K., Araki, K., Takayama, C., Inoue, Y., Yagi, T., Aizawa, S., and Mishina, M. (1995). Reduced spontaneous activity of mice defective in the epsilon 4 subunit of the NMDA receptor channel. Brain Res. Mol. Brain Res. *33*, 61–71.

Jeffery, K.J., Donnett, J.G., and O'Keefe, J. (1995). Medial septal control of theta-correlated unit firing in the entorhinal cortex of awake rats. Neuroreport *6*, 2166–2170.

Kamondi, A., Acsady, L., Wang, X.J., and Buzsaki, G. (1998). Theta oscillations in somata and dendrites of hippocampal pyramidal cells in vivo: Activity-dependent phase-precession of action potentials. Hippocampus *8*, 244–261.

Kauer, J.A., Malenka, R.C., and Nicoll, R.A. (1988). NMDA application potentiates synaptic transmission in the hippocampus. Nature *334*, 250–252.

Kawabe, K., Ichitani, Y., and Iwasaki, T. (1998). Effects of intrahippocampal AP5 treatment on radial-arm maze performance in rats. Brain Res. *781*, 300–306.

Kiss, J., Buzsaki, G., Morrow, J.S., Glantz, S.B., and Leranth, C. (1996). Entorhinal cortical innervation of parvalbumin-containing neurons (Basket and Chandelier cells) in the rat Ammon's horn. Hippocampus *6*, 239–246.

Klausberger, T., Marton, L.F., O'Neill, J., Huck, J.H., Dalezios, Y., Fuentealba, P., Suen, W.Y., Papp, E., Kaneko, T., Watanabe, M., et al. (2005). Complementary roles of cholecystokinin- and parvalbumin-expressing GABAergic neurons in hippocampal network oscillations. J. Neurosci. *25*, 9782–9793.

Kocsis, B., Bragin, A., and Buzsaki, G. (1999). Interdependence of multiple theta generators in the hippocampus: A partial coherence analysis. J. Neurosci. *19*, 6200–6212.

Kramis, R., Vanderwolf, C.H., and Bland, B.H. (1975). Two types of hippocampal rhythmical slow activity in both the rabbit and the rat: Relations to behavior and effects of atropine, diethyl ether, urethane, and pentobarbital. Exp. Neurol. *49*, 58–85.

Lee, I., and Kesner, R.P. (2002). Differential contribution of NMDA receptors in hippocampal subregions to spatial working memory. Nat. Neurosci. *5*, 162–168.

Lewis, D.A., Hashimoto, T., and Volk, D.W. (2005). Cortical inhibitory neurons and schizophrenia. Nat. Rev. Neurosci. *6*, 312–324.

Li, X.G., Somogyi, P., Tepper, J.M., and Buzsaki, G. (1992). Axonal and dendritic arborization of an intracellularly labeled chandelier cell in the CA1 region of rat hippocampus. Exp. Brain Res. *90*, 519–525.

Lisman, J. (2005). The theta/gamma discrete phase code occurring during the hippocampal phase precession may be a more general brain coding scheme. Hippocampus *15*, 913–922.

Lisman, J.E., and Idiart, M.A. (1995). Storage of 7 +/− 2 short-term memories in oscillatory subcycles. Science *267*, 1512–1515.

Lisman, J., and Buzsaki, G. (2008). A neural coding scheme formed by the combined function of gamma and theta oscillations. Schizophr. Bull. *34*, 974–980.

Lodge, D.J., Behrens, M.M., and Grace, A.A. (2009). A loss of parvalbumin-containing interneurons is associated with diminished oscillatory activity in an animal model of schizophrenia. J. Neurosci. *29*, 2344–2354.

Ma, J., and Leung, L.S. (2000). Relation between hippocampal gamma waves and behavioral disturbances induced by phencyclidine and methamphetamine. Behav. Brain Res. *111*, 1–11.

McHugh, T.J., Blum, K.I., Tsien, J.Z., Tonegawa, S., and Wilson, M.A. (1996). Impaired hippocampal representation of space in CA1-specific NMDAR1 knockout mice. Cell *87*, 1339–1349.

McHugh, T.J., Jones, M.W., Quinn, J.J., Balthasar, N., Coppari, R., Elmquist, J.K., Lowell, B.B., Fanselow, M.S., Wilson, M.A., and Tonegawa, S. (2007). Dentate gyrus NMDA receptors mediate rapid pattern separation in the hippocampal network. Science *317*, 94–99.

Mitchell, S.J., Rawlins, J.N., Steward, O., and Olton, D.S. (1982). Medial septal area lesions disrupt theta rhythm and cholinergic staining in medial entorhinal cortex and produce impaired radial arm maze behavior in rats. J. Neurosci. *2*, 292–302.

Mizuseki, K., Sirota, A., Pastalkova, E., and Buzsaki, G. (2009). Theta oscillations provide temporal windows for local circuit computation in the entorhinal-hippocampal loop. Neuron *64*, 267–280.

Mohn, A.R., Gainetdinov, R.R., Caron, M.G., and Koller, B.H. (1999). Mice with reduced NMDA receptor expression display behaviors related to schizophrenia. Cell *98*, 427–436.

Montgomery, S.M., Sirota, A., and Buzsaki, G. (2008). Theta and gamma coordination of hippocampal networks during waking and rapid eye movement sleep. J. Neurosci. *28*, 6731–6741.

Monyer, H., Sprengel, R., Schoepfer, R., Herb, A., Higuchi, M., Lomeli, H., Burnashev, N., Sakmann, B., and Seeburg, P.H. (1992). Heteromeric NMDA receptors: Molecular and functional distinction of subtypes. Science *256*, 1217–1221.

Morris, R.G., Anderson, E., Lynch, G.S., and Baudry, M. (1986). Selective impairment of learning and blockade of long-term potentiation by an N-methyl-D-aspartate receptor antagonist, AP5. Nature *319*, 774–776.

Nakazawa, K., Quirk, M.C., Chitwood, R.A., Watanabe, M., Yeckel, M.F., Sun, L.D., Kato, A., Carr, C.A., Johnston, D., Wilson, M.A., and Tonegawa, S. (2002). Requirement for hippocampal CA3 NMDA receptors in associative memory recall. Science *297*, 211–218.

Nakazawa, K., Sun, L.D., Quirk, M.C., Rondi-Reig, L., Wilson, M.A., and Tonegawa, S. (2003). Hippocampal CA3 NMDA receptors are crucial for memory acquisition of one-time experience. Neuron *38*, 305–315.

Nakazawa, K., McHugh, T.J., Wilson, M.A., and Tonegawa, S. (2004). NMDA receptors, place cells and hippocampal spatial memory. Nat. Rev. Neurosci. *5*, 361–372.

Niewoehner, B., Single, F.N., Hvalby, O., Jensen, V., Meyer zum Alten Borgloh, S., Seeburg, P.H., Rawlins, J.N., Sprengel, R., and Bannerman, D.M. (2007). Impaired spatial working memory but spared spatial reference memory following functional loss of NMDA receptors in the dentate gyrus. Eur. J. Neurosci. *25*, 837–846.

O'Keefe, J., and Nadel, L. (1978). The Hippocampus as a Cognitive Map (Oxford, UK: Oxford University Press).

Pawelzik, H., Hughes, D.I., and Thomson, A.M. (2002). Physiological and morphological diversity of immunocytochemically defined parvalbumin- and cholecystokinin-positive interneurones in CA1 of the adult rat hippocampus. J. Comp. Neurol. *443*, 346–367.

Petsche, H., Stumpf, C., and Gogolak, G. (1962). The significance of the rabbit's septum as a relay station between the midbrain and the hippocampus. I. The control of hippocampus arousal activity by the septum cells. Electroencephalogr. Clin. Neurophysiol. *14*, 202–211.

Racz, A., Ponomarenko, A.A., Fuchs, E.C., and Monyer, H. (2009). Augmented hippocampal ripple oscillations in mice with reduced fast excitation onto parvalbumin-positive cells. J. Neurosci. *29*, 2563–2568.

Raghavachari, S., Kahana, M.J., Rizzuto, D.S., Caplan, J.B., Kirschen, M.P., Bourgeois, B., Madsen, J.R., and Lisman, J.E. (2001). Gating of human theta oscillations by a working memory task. J. Neurosci. *21*, 3175–3183.

Rampon, C., Tang, Y.P., Goodhouse, J., Shimizu, E., Kyin, M., and Tsien, J.Z. (2000). Enrichment induces structural changes and recovery from nonspatial memory deficits in CA1 NMDAR1-knockout mice. Nat. Neurosci. *3*, 238–244.

Rawlins, J.N., and Olton, D.S. (1982). The septo-hippocampal system and cognitive mapping. Behav. Brain Res. *5*, 331–358.

Roopun, A.K., Kramer, M.A., Carracedo, L.M., Kaiser, M., Davies, C.H., Traub, R.D., Kopell, N.J., and Whittington, M.A. (2008). Temporal interactions between cortical rhythms. Front Neurosci *2*, 145–154.

Rotstein, H.G., Pervouchine, D.D., Acker, C.D., Gillies, M.J., White, J.A., Buhl, E.H., Whittington, M.A., and Kopell, N. (2005). Slow and fast inhibition and an H-current interact to create a theta rhythm in a model of CA1 interneuron network. J. Neurophysiol. *94*, 1509–1518.

Sakimura, K., Kutsuwada, T., Ito, I., Manabe, T., Takayama, C., Kushiya, E., Yagi, T., Aizawa, S., Inoue, Y., Sugiyama, H., et al. (1995). Reduced hippocampal LTP and spatial learning in mice lacking NMDA receptor epsilon 1 subunit. Nature *373*, 151–155.

Shin, J., Kim, D., Bianchi, R., Wong, R.K., and Shin, H.S. (2005). Genetic dissection of theta rhythm heterogeneity in mice. Proc. Natl. Acad. Sci. USA *102*, 18165–18170.

Sik, A., Penttonen, M., Ylinen, A., and Buzsaki, G. (1995). Hippocampal CA1 interneurons: An in vivo intracellular labeling study. J. Neurosci. *15*, 6651–6665.

Sirota, A., Montgomery, S., Fujisawa, S., Isomura, Y., Zugaro, M., and Buzsaki, G. (2008). Entrainment of neocortical neurons and gamma oscillations by the hippocampal theta rhythm. Neuron *60*, 683–697.

Sohal, V.S., Zhang, F., Yizhar, O., and Deisseroth, K. (2009). Parvalbumin neurons and gamma rhythms enhance cortical circuit performance. Nature *459*, 698–702.

Soltesz, I., and Deschenes, M. (1993). Low- and high-frequency membrane potential oscillations during theta activity in CA1 and CA3 pyramidal neurons of the rat hippocampus under ketamine-xylazine anesthesia. J. Neurophysiol. *70*, 97–116.

Stewart, M., and Fox, S.E. (1990). Do septal neurons pace the hippocampal theta rhythm? Trends Neurosci. *13*, 163–168.

Tort, A.B., Kramer, M.A., Thorn, C., Gibson, D.J., Kubota, Y., Graybiel, A.M., and Kopell, N.J. (2008). Dynamic cross-frequency couplings of local field potential oscillations in rat striatum and hippocampus during performance of a T-maze task. Proc. Natl. Acad. Sci. USA *105*, 20517–20522.

Vanderwolf, C.H. (1969). Hippocampal electrical activity and voluntary movement in the rat. Electroencephalogr. Clin. Neurophysiol. *26*, 407–418.

Vanderwolf, C.H., and Leung, L.S. (1983). Hippocampal rhythmical slow activity: A brief history and the effects of entorhinal lesions and phencyclidine. In The Neurobiology of the Hippocampus, W. Seifert, ed. (London: Academic Press), pp. 275–302.

von Engelhardt, J., Doganci, B., Jensen, V., Hvalby, O., Gongrich, C., Taylor, A., Barkus, C., Sanderson, D.J., Rawlins, J.N., Seeburg, P.H., et al. (2008). Contribution of hippocampal and extra-hippocampal NR2B-containing NMDA receptors to performance on spatial learning tasks. Neuron *60*, 846–860.

Wilson, M.A., and McNaughton, B.L. (1993). Dynamics of the hippocampal ensemble code for space. Science *261*, 1055–1058.

Winson, J. (1974). Patterns of hippocampal theta rhythm in the freely moving rat. Electroencephalogr. Clin. Neurophysiol. *36*, 291–301.

Wulff, P., Ponomarenko, A.A., Bartos, M., Korotkova, T.M., Fuchs, E.C., Bahner, F., Both, M., Tort, A.B., Kopell, N.J., Wisden, W., and Monyer, H. (2009). Hippocampal theta rhythm and its coupling with gamma oscillations require fast inhibition onto parvalbumin-positive interneurons. Proc. Natl. Acad. Sci. USA *106*, 3561–3566.